



**HAL**  
open science

## Elucidating 2D Charge-Density-Wave atomic structure in an MXchain by the 3D- $\Delta$ Pair Distribution Function method

Laurent Guérin, Takefumi Yoshida, Edoardo Zatterin, Arkadiy Simonov, Dmitry Chernyshov, Hiroaki Iguchi, Bertrand Toudic, Shinya Takaishi, Masahiro Yamashita

### ► To cite this version:

Laurent Guérin, Takefumi Yoshida, Edoardo Zatterin, Arkadiy Simonov, Dmitry Chernyshov, et al.. Elucidating 2D Charge-Density-Wave atomic structure in an MXchain by the 3D- $\Delta$ Pair Distribution Function method. *ChemPhysChem*, 2022, 23 (6), pp.e202100857. 10.1002/cphc.202100857 . hal-03550904

HAL Id: hal-03550904

<https://hal.science/hal-03550904>

Submitted on 1 Apr 2022

**HAL** is a multi-disciplinary open access archive for the deposit and dissemination of scientific research documents, whether they are published or not. The documents may come from teaching and research institutions in France or abroad, or from public or private research centers.

L'archive ouverte pluridisciplinaire **HAL**, est destinée au dépôt et à la diffusion de documents scientifiques de niveau recherche, publiés ou non, émanant des établissements d'enseignement et de recherche français ou étrangers, des laboratoires publics ou privés.



Distributed under a Creative Commons Attribution - NonCommercial 4.0 International License

# Elucidating 2D Charge-Density-Wave atomic structure in an MX-chain by the 3D- $\Delta$ Pair Distribution Function method

Laurent Guérin,<sup>\*1</sup> Takefumi Yoshida,<sup>\*2</sup> Edoardo Zatterin,<sup>1,3</sup> Arkadiy Simonov,<sup>1,4</sup> Dmitry Chernyshov,<sup>5</sup> Hiroaki Iguchi,<sup>2</sup> Bertrand Toudic,<sup>1</sup> Shinya Takaishi,<sup>2</sup> Masahiro Yamashita<sup>2,6</sup>

- [1] Dr. L. Guérin, Dr. E. Zatterin, Dr. A. Simonov, Dr. B. Toudic  
Univ Rennes, CNRS, IPR (Institut de Physique de Rennes) - UMR 6251, F-35000 Rennes, France .  
E-mail: laurent.guerin@univ-rennes1.fr
- [2] Dr. T. Yoshida, Dr. H. Iguchi, Prof. M. Yamashita, Dr. Shinya Takaishi  
Department of Chemistry, Graduate School of Science, Tohoku University, 6-3 Aramaki-Aza-Aoba, Aoba-Ku, Sendai 980-8578, Japan.  
E-mail: takefumi.yoshida@uec.ac.jp
- [3] Dr. E. Zatterin  
ESRF–The European Synchrotron, BM31, 71 Avenue des Martyrs, Grenoble 38000, France.
- [4] Dr. A. Simonov  
Materials Department, ETH Zürich, Vladimir-Prelog-Weg 1-5/10, 8093 Zürich, Switzerland.
- [5] Dr. D. Chernyshov  
Swiss- Norwegian BeamLines at the ESRF, 71 Avenue des Martyrs, Grenoble 38000, France.
- [6] Prof. M. Yamashita  
School of Materials Science and Engineering, Nankai University, Tianjin 300350, China.

Supporting information for this article is given via a link at the end of the document.

**Abstract:** Many solids, particularly low-dimensional systems, exhibit charge density waves (CDWs). In one dimension, charge density waves are well understood, but in two dimensions, their structure and their origin are difficult to reveal. Here, the 2D Charge-Density-Wave atomic structure and stabilization mechanism in the bromide-bridged Pd compound  $[\text{Pd}(\text{cptn})_2\text{Br}]_2\text{Br}_2$  (cptn = 1*R*,2*R*-diaminocyclopentane) is investigated by means of single-crystal X-ray diffraction employing the 3D- $\Delta$ Pair Distribution Function (3D- $\Delta$ PDF) method. Analysis of the diffuse scattering using 3D- $\Delta$ PDF shows that a 2D-CDW is stabilized by a hydrogen-bonding network between  $\text{Br}^-$  counteranion and the amine ( $\text{NH}_2$ ) group of the cptn in-plane ligand, and that 3D ordering is prevented due to a weak plane to plane correlation. We extract the effective displacements of the atoms describing the atomic structure quantitatively and discuss the stabilization mechanism of the 2D-CDW. Our study provides a method to identify and measure the key interaction responsible for the dimensionality and stability of the CDW that can help further progress of rational design.

## Introduction

In the field of molecular-based conductors, investigations of diffuse scattering have played a major role.[1,2] Indeed, the first diffuse scattering experiments on TTF-TCNQ[3] paved the way for the discovery of numerous original structural phases in molecular conductors.[4] Due to the so-called Peierls instability that prevails in 1D physics, a resulting periodic modulation of the electron density named Charge-Density-Wave (CDW), can be stabilized, and is associated with a periodic lattice distortion. A very large number of studies in the last 50 years have been conducted in order to understand the different mechanisms of stabilization of the CDW and to control its dimensionality, either using chemical design or via the manipulation of external parameters such as temperature, pressure or light.[5-10] Bechgaard salt, Fabre salts or dmit salts compose such a playground. Quasi-one-dimensional halogen-bridged metal complexes, so-called MX-Chains, are also suitable candidates to understand the correlation between the lattice and the electrons

responsible for the CDW order. MX-Chains have an isolated one-dimensional (1D) electronic system composed of  $d_{z^2}$  orbital of metal ions (M) and  $p_z$  orbital of bridging halide ions (X) (Figure S1).[11] These electronic states are well explained by the extended Peierls-Hubbard model, where the transfer integral ( $t$ ), the on-site and nearest neighbor-site Coulomb repulsion ( $U$  and  $V$ , respectively), and the electron-lattice interaction ( $S$ ) strongly compete with each other. The very large majority of Pd, and Pt complexes, which have a  $-\text{X}\cdots\text{M}^{\text{II}}\cdots\text{X}-\text{M}^{\text{IV}}-\text{X}\cdots$  Peierls distorted 1D structure, are in a mixed-valence charge-density-wave (MV-CDW) state because of a small  $U$  value ( $S > U$ ) (Figure S2).[12] This mixed-valence state is accompanied by a strong dimerization along the chain, with two competing CDW ground states (A and B in Figure 1a) that can be easily characterized using single-crystal X-ray diffraction.[11] However, recently some Pd complexes which show a CDW-to-Mott-Hubbard (MH) phase transition where the decrement of Pd...Pd distances at low temperature reduce  $S$  value (while the  $U$  value remains almost constant), thus stabilizing the MH state, have been reported.[13] In such a case, at variance with CDW, the X-M-X bonds are completely symmetric. In particular,  $[\text{Pd}(\text{cptn})_2\text{Br}]_2\text{Br}_2$  (cptn = 1*R*,2*R*-diaminocyclopentane) was shown to be the only reported system among organic molecular solids, where  $\mu\text{m}$ -order CDW and MH domains coexist in a wide temperature range although the stabilization mechanisms were not revealed.[14] Very convincing evidence of the Peierls instability was provided by diffuse scattering since the low-dimensional character of the CDW can be spotted by the diffuse scattering out of the Bragg peaks.[2] However, up to now, most parts of the analysis concerning diffuse scattering originating from CDWs were qualitative, with no quantitative information on the displacement of atoms and therefore on the real structure of the CDW state. Analysis of the local structure requires the Fourier Transform of the intensity of the diffuse scattering, which contains the information on the pair correlation function of the disorder. It should be mentioned that a pioneering handmade approach was made some years ago considering short-range ordering in a Ni-Pd-based MX-Chain compound.[15] These types of studies require single crystals,

intense X-rays and a zero-noise detector with ultra-high dynamic range. These experimental conditions are now available thanks to advent of bright synchrotron radiations sources and large area pixel photon-counting detectors. In this study, we characterize the stabilization mechanism of the macroscopic CDW domains measuring X-ray diffuse scattering patterns and interpreting these patterns via three-dimensional difference pair distribution function (3D- $\Delta$ PDF) analysis and refinement of disorder models against single-crystal diffuse scattering data (Yell). We extract the effective displacements of the atoms describing the CDW atomic structure quantitatively by this way.

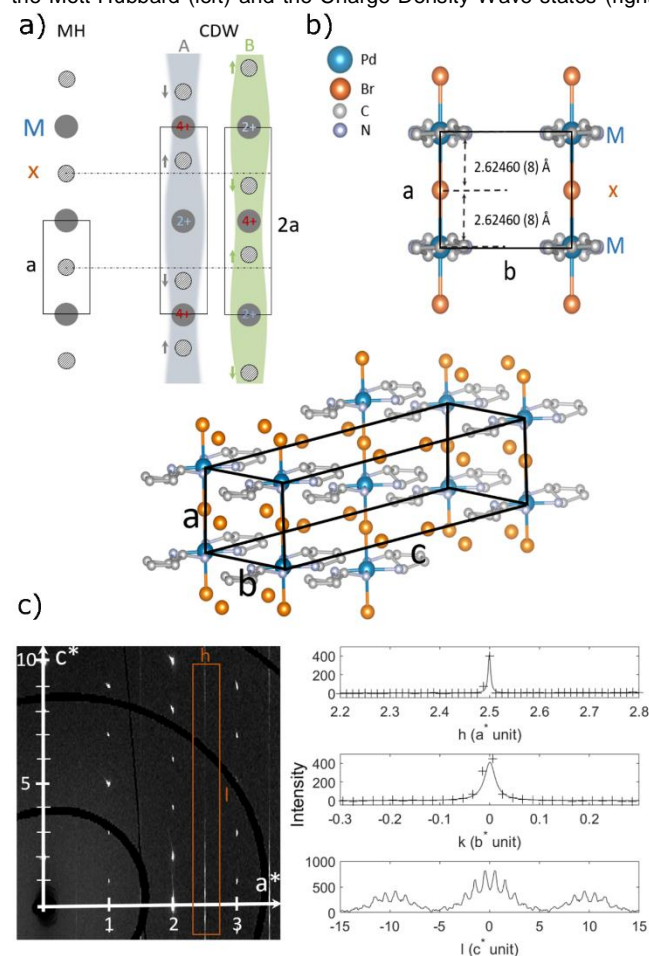
## Results and Discussion

**Determination of the average structure.** Single-crystal  $[\text{Pd}(\text{cptn})_2\text{Br}]\text{Br}_2$  samples were grown by the electrochemical oxidation method and synthesized from the same cptn enantiomer (1*R*,2*R*-diaminocyclopentane). A set of single crystals of  $[\text{Pd}(\text{cptn})_2\text{Br}]\text{Br}_2$  of plate-like shape, with lateral dimensions of some hundreds of  $\mu\text{m}$ , were studied by X-Ray diffraction at 260 K to investigate their crystal structure. X-ray measurements were carried out at the Swiss Norwegian Beamline BM01 at the European Synchrotron Research Facility using monochromatized X-rays with  $\lambda = 0.6973 \text{ \AA}$ . 900 images with 0.4 s exposure times and  $0.4^\circ$  step size were collected with a Pilatus2M detector located 247 mm downstream of the crystal.[16] Structure solution and refinement using the software Jana yielded an orthorhombic structure of space group *I*222 with the lattice parameters  $a = 5.249 \text{ \AA}$ ,  $b = 6.972 \text{ \AA}$ ,  $c = 22.711 \text{ \AA}$ . As illustrated in Figure 1b (also Figure S3-4), the structure consists of a body-centered arrangement of  $[\text{Pd}(\text{cptn})_2\text{Br}]\text{Br}_2$  chains. A single chain is composed of an alternation of  $\text{Pd}(\text{cptn})_2$  units bridged by Br ions along the *a* axis; the amine ( $\text{NH}_2$ ) groups of the cptn ligand provide cohesion between chains in the *b* direction through hydrogen bonds formed with the  $\text{Br}^-$  counteranions (H bond length = 2.65  $\text{\AA}$ ). The cptn ligands extend from each chain in the *c* direction. The space group *I*222 was discriminated from its crystallographically indistinguishable counterpart *I**mmm* on the basis of the chemical reason that the enantiopure ligand violates *mmm* symmetry. The important observation is that the Pd-Br-Pd distance was symmetric, and no sign of dimerization was observed. There is no evidence of a CDW organization regarding the average structure from this single crystal structural analysis. This appears to be in contradiction with theory and previous STM and Raman measurements.[14]

**Analysis of the diffuse scattering.** A representative (*h* 0 *l*) section of the three-dimensional scattering pattern is shown in Figure. 1c. It contains weak but highly structured diffuse scattering, which is the signature of the strongly correlated disorder and is determined by spatial fluctuations in the structure.[17-20] A set of streaks parallel to the  $c^*$  axis and perpendicular to the ( $a^*$ ,  $b^*$ ) plane are observed, suggesting the existence of a two-dimensional (*a*, *b*) ordering in real space with disorder along the *c* direction. Correlation lengths of 2100  $\text{\AA}$  (400 unit cells) and 480  $\text{\AA}$  (70 unit cells) in the *a* and *b* crystallographic directions, respectively, were extracted from a Lorentzian fit of the profile of the diffuse streaks along the  $a^*$  and  $b^*$  directions. The streaks intersect the *H* direction at half-integer values, while along the *K* direction only integer values are met. This means that the ordering

phenomenon results in a double periodicity in terms of structural displacements along *a* with respect to the average structure defined by the Bragg peaks position. On the other hand, the same periodicity between average and real structure occurs in the *b* direction. Individual (*a*, *b*) planes in the crystal are composed of chains with a double periodicity compared to the average structure, with each neighboring chain in the *b* direction being ordered in phase. Thus, one can say that a long-range order occurs in individual planes. The fundamental question is how this order can be related to a CDW state.

**Figure 1.** X-ray analysis of  $\text{Pd}(\text{cptn})_2\text{Br}]\text{Br}_2$  MX chains a) Schematic representation in halogen-bridged metal compounds (MX chains) of the Mott Hubbard (left) and the Charge Density Wave states (right)

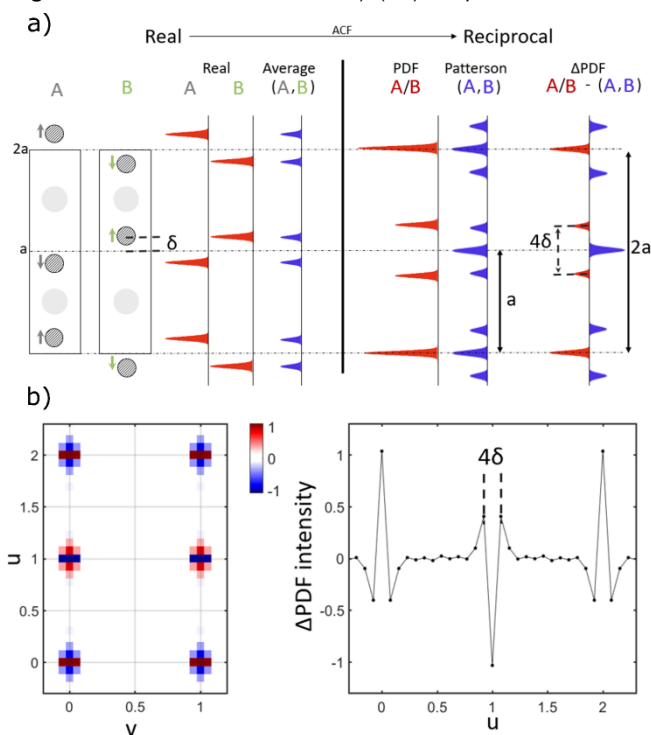


showing the two competitive ground states (A and B). Note the cell doubling along *a* associated to the dimerization of the halogen ion X in the CDW state. b) the orthorhombic structure of the MX-Chain compound  $\text{Pd}(\text{cptn})_2\text{Br}]\text{Br}_2$ . c) (left) reconstructed (*h* 0 *l*) reciprocal plane shows  $c^*$  diffuse streaks at half integer values of  $a^*$ . (right) ( $h = 2.5$ ) streak profiles and their lorentzian fit.

**A 2D-CDW is evidenced by the 3D- $\Delta$ PDF method.** The three-dimensional difference pair distribution function (3D- $\Delta$ PDF) contains information on the self-correlation function of the short-range ordering as measured away from the Bragg peaks on single crystals.[21-25] To illustrate this method, we introduce a 1D - model of dimerization (Figure 2a). We considered a real crystal composed of two different structures A and B generated by anti-phase displacement ( $\delta$ ) of nearest atoms, each structure related

to the other by a one-half translation along  $a$ . Each structure has an equal probability, and no correlation is assumed, so the “real” crystal is highly disordered. Electron density peaks of the average structure are located at the position of the electron density peaks of the two real structures giving rise to a periodicity of half the real periodicity. Model diffraction patterns can be obtained from the autocorrelation function of the electron density known as the PDF and the Patterson calculated from the real structure and the average structure, respectively. The  $\Delta$ PDF is the difference between the PDF and the Patterson function. In the specific case of dimerization, we observe a distinct repetition of positive-negative-positive and negative-positive-negative peaks, with direct and inverse profiles. The distance  $4\delta$  within these profiles is directly related to the displacement of the dimerization. Its periodicity, the same as the real structure, is twice the periodicity of the average structure.

**Figure 2.**  $\Delta$ PDF of MX-Chains. a) (left) simple model of  $a + \delta$



dimerization along  $a$  with equal probability of A and B atomic configurations. Electron density of the individual A, B atomic positions (real structure) and the average structure. (right) Associated autocorrelated function (ACF) of the A/B structure (PDF), of the average (Patterson) and their difference ( $\Delta$ PDF = PDF-Patterson). Note the cell doubling in the  $\Delta$ PDF. The distance of two characteristic positive peaks in the  $\Delta$ PDF corresponds to  $4\delta$ . b) experimental normalized  $\Delta$ PDF of the  $(a,b)$  plane (left) and its profile along  $a$  (right). The displacement is  $\delta = 0.038a = 0.2 \text{ \AA}$

The inverse Fourier transform of the normalized diffuse scattering function yields the 3D- $\Delta$ PDF,[21] a three-dimensional real space reconstruction consisting of voxels. The position of each voxel with respect to the center of the  $\Delta$ PDF represents an interatomic vector; the normalized intensity of a voxel corresponds to the probability of that specific interatomic vector being found in the real structure rather than the average one. That is, positive intensities in the 3D- $\Delta$ PDF represent interatomic

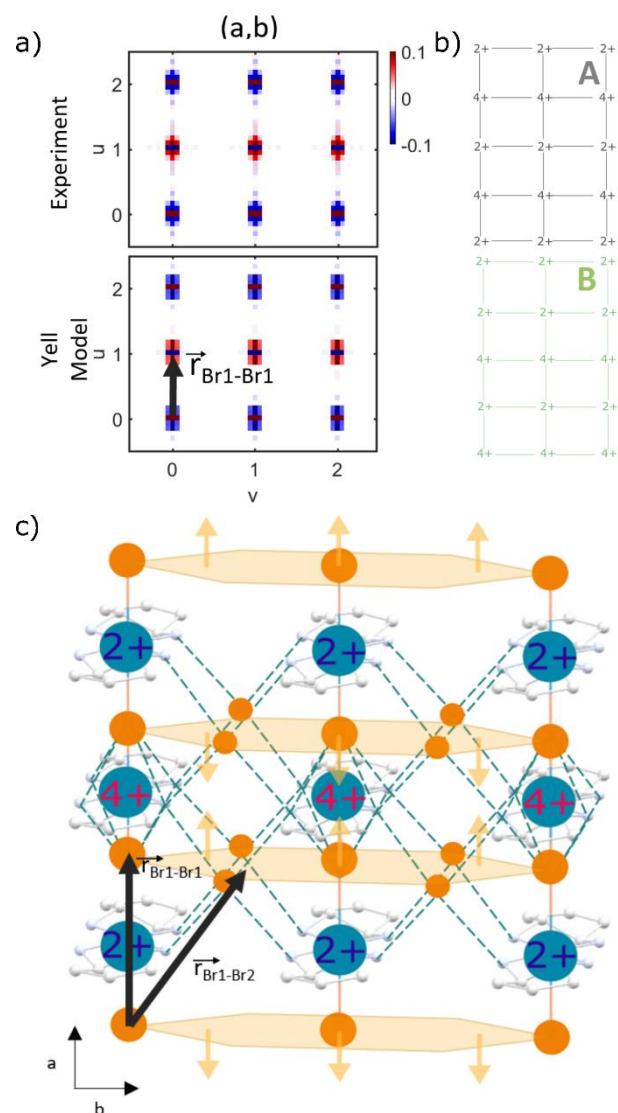
vectors, which are more probable to be found in the real than in the average structure, and vice versa for negative intensities. The quality and the resolution of the  $\Delta$ PDF are defined by the number of streaks collected and their intensities compared to the background, which is improved drastically with the use of a synchrotron and a pixel detector.[16] The size of the present  $\Delta$ PDF ( $26 \times 18 \times 800$  voxels) and the corresponding voxel size ( $0.40 \times 0.58 \times 0.03 \text{ \AA}$ ) stems from the data acquisition strategy and the integration procedure. The reciprocal volume of diffuse streaks was merged into 1D pixel arrays to increase the data statistics (Figure 1c), thus implicitly assuming perfect correlation in the  $a^*$  and  $b^*$  directions. Figure 2b shows a section of the  $\Delta$ PDF corresponding to the  $(u, v, 0)$  plane. As already discussed for the diffuse scattering, cell doubling along the chain ( $a$  direction) is observed in the  $\Delta$ PDF while the periodicity perpendicular to the chain along the  $b$  direction remains unvaried. The typical pattern of dimerization is clearly revealed in the profile along the  $a$  direction corresponding to an overall displacement of  $\delta = 0.2 \text{ \AA}$ .

#### Determination of the atomic structure of the CDW and its stabilization mechanism.

The software Yell[26] allows for the specification of a disorder model, starting from the average structure of the crystal that we determined previously. A displacive model using 3 parameters corresponding to a displacement along a direction of the  $\text{Br}^-$  bridging anion (Br1), the  $\text{Br}^-$  counteranion (Br2) and the terminal carbon atom of cptn ligand (so-called C atom) is used to generate a  $\Delta$ PDF (Figure 3a, 4a and Figure S6). This function is refined against the experimentally obtained one. A displacement of  $\Delta = 0.136 \text{ \AA}$  of the Br bridging atom along the chain is obtained. It has been established that the distortion parameter defined as  $d = 2\Delta/a$ , bears a linear relationship to  $a : d = 0.165 a - 0.81$ . [27] The obtained value of  $d = 2\Delta/a = 0.052$  for  $a = 5.25 \text{ \AA}$  is in perfect agreement with other Pd-based MX chains found in a CDW state, confirming the CDW nature of the electronic state (Figure S7). [27] The analysis of the  $\Delta$ PDF and width of the diffuse streaks indicate that the  $(a, b)$  plane consists of long-range ordered dimerized chains. Because of the observed displacement of the Br bridging atom associated with the Peierls distortion, we conclude that the electronic state of an individual  $(a, b)$  plane is a two-dimensional CDW state (figure 3b). In Figure 4a, the  $(0, v, w)$  plane shows strong positive peaks corresponding to the interatomic vector between Br1 and Br2 (Figure 3a). It indicates that the Br1 and Br2 atoms are displaced in phase in the  $a$  direction. The counteranion Br2 displaces in phase with Br1. The magnitude of the displacement, equal to  $0.035 \text{ \AA}$  is about 4 times less than of the Br bridging atom. Looking at the average structure, one can notice that the Br bridging and counteranions are connected by a hydrogen-bonding network (Figure 3c and S5). In consequence to the Br2 displacement, the hydrogen bond length shows two different value depending on the valence order  $2.61 \text{ \AA}$  for 2+ and  $2.69 \text{ \AA}$  for 4+. Based on those results, both intrachain and interchain correlations can be understood, and the mixed-valence 2D CDW structure discerned, as is sketched in Figure 3c. In the chain,  $U$  is affected by the electrostatic / ligand field around the  $d_{z^2}$  orbital. It appears that the influence of the axial ligand of Br anion is dominant, and the in-plane ligand of cptn is irrelevant. The ligand field affects the value of the on-site Coulomb repulsion  $U$  on the metal ion and stimulates the formation of the CDW mixed-valence state in the chain via a Peierls distortion. In the interchain, once a dimerization starts

occurring locally in the  $a$  direction (either A or B type) along the chain axis, it is easily propagated in the  $b$  direction due to the presence of the H-bonds (which provides interchain cohesion in the  $b$  direction) and mediated by the  $\text{Br}^-$  counteranions. Thus, once one chain has dimerized in a certain way, all the chains contained in the same  $(a, b)$  plane dimerize in the same way, and a 2D-CDW state is stabilized (Figure 3b).

**Figure 3.** a) Yell Disorder model compared to the experimental 3D- $\Delta$ PDF. The normalized experimental  $\Delta$ PDF of the  $(u, v, 0)$  plane and



that calculated from a disorder model. Interatomic vectors corresponding to strong  $\Delta$ PDF peaks are represented in the  $\Delta$ PDF and in the average structure (see also Figure. 4). Note the rather good agreement of the experimental data with the theoretical model. The negative correlation corresponding to Br1-Br1 is a signature of the dimerization along the chain. b) a schematic diagram of the two types of 2D CDW arrangements (A and B) c) The mixed-valence 2D CDW schematic structure in the  $(a, b)$  plane. The hydrogen-bonding network (green dashed lines) is shown. Yellow arrows represent the dimerization of the Br1-Br2 molecules along the chain direction.

**Characterization of the plane to plane correlation.** The  $(u, 0, w)$  and  $(0, v, w)$  sections shown in Figure 4a further allow the interpretation of the correlated disorder between the two-

dimensional CDW  $(a, b)$  planes stacked and shuffled along the orthogonal direction. Because of the degenerate ground state of the CDW state (A/B in Figure 1a and 3b) and weak plane-to-plane interaction, disorder appears along the  $c$  direction. Both the  $(a, c)$  and  $(b, c)$  section of the  $\Delta$ PDF show opposite signs of features for adjacent unit cells along  $c$  direction, indicating negative correlation between adjacent  $(a, b)$  plane. Experimentally, this negative correlation originating from the one-half  $c^*$  periodicity manifests itself as sharper peaks in the intensity profile of the streaks (Figure 1c). One can then assume a small displacement of the Br1 and Br2 atoms as derived from the first model, apply it to entire  $(a, b)$  planes, and derive a substitutional model in order to investigate the correlations along the  $c$  direction. The obtained joint probability  $P(A/B)$  that planes separated by a given vector in  $c$  are ordered in a different way is found to be equal to 0.54. This indicates that there is not a complete disorder along  $c$  (which would be characterized by a probability 0.5) (Figure 4d). The 2D-CDW of a given  $(a, b)$  plane tends to slightly order in an anti-phase manner, with the CDW being shifted by  $a/2$  between two adjacent planes with a very short correlation length. The value of this length was estimated from the fit of the sharper peaks along  $c$  and was found to be equal to 52 Å (2.3 unit cells). This anti-phase process is known as the Coulomb coupling and is illustrated schematically in figure 4c. This mechanism is usually invoked to account for the CDW transverse ordering in TTF-TCNQ and related compounds where these interactions make the diffuse scattering condense in commensurate positions at the phase transition.[2] Very weak and positive correlations between the terminal carbon atom of the cptn ligand (C) and the  $\text{Br}^-$  counteranion (Br2) are also present in the model. Those two atoms tend to displace in phase (as illustrated in Figure 4b), resulting in a small plane to plane correlation, preventing the stabilization of a 3D-CDW order. It is not surprising that the involved chemical bond must be very weak as its bond length is about 3.6 Å. It also seems to act as a chemical press and influence the valence of the metal in the chain.

**Temperature dependence.**  $\mu\text{m}$ -order CDW and MH domains coexist in a wide temperature range with a possible phase transition at 120K.[14] In order to investigate the temperature dependence of the CDW correlation length, we performed several measurements from 100 K to room temperature. The intensity of the diffuse scatterings seems to gradually weaken upon cooling and mostly disappeared at 100 K, indicating that the electronic state is changing from CDW to MH state gradually (Figure S8). The reproducibility was poor due to X-ray damage after few minutes. We observed no temperature dependence of the correlation length. There was no evidence of condensation of diffuse planes to Bragg peaks as observed in other molecular based conductors [2,6,10]. It indicates that the CDW order is 2D for any temperature as the strong hydrogen bonding network anchors the charge order to the chains and the weak plane to plane correlation must prevent the formation of a 3D ordering.

## Discussion

The present study has demonstrated the great power of the 3D- $\Delta$ PDF method in analyzing diffuse scattering data and provide insights into the disorder presents inside a material. The absence

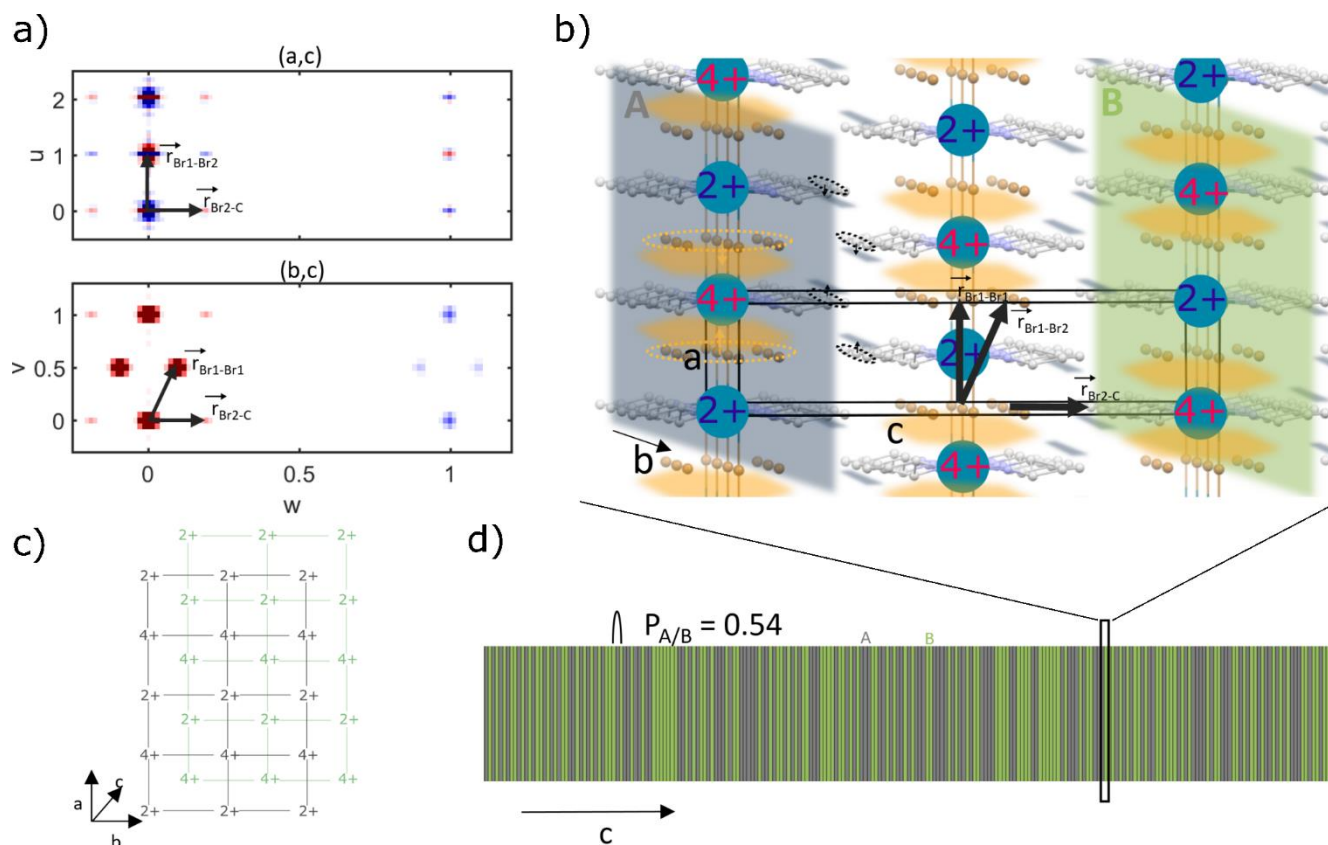


**Figure 4.** a) Experimental 3D- $\Delta$ PDF of  $(u, 0, w)$  and  $(0, v, w)$ . Interatomic vectors corresponding to strong  $\Delta$ PDF peaks are represented in the  $\Delta$ PDF and in the average structure. Negative correlation is observed at  $w = 1$  and corresponds to anti-phase ordering along the  $c$  direction. b) The mixed-valence 2D CDW schematic structure along the  $c$  direction. The interatomic vector between bromide counteranion and terminal carbon atom (black arrow) and the displacement of bromine atoms (yellow glooms) and of terminal carbon atom of cptn ligand (yellow glooms and arrows) are represented. Note the  $a/2$  phase shift of the CDW from plane to plane. c) Schematic structure of stacking of two 2D CDW planes d) Schematic representation of A/B ordering along the  $c$  direction. The joint probability  $P_{A/B}$  is found to be 0.54, complete disorder corresponding to 0.5. Alternation of A/B planes is more probable. ( $P_{A/B} = 0.60$  was chosen in this schematic representation to enhance the anti-phase ordering)

of superstructure Bragg peaks and the wrong assumption that the crystal structure corresponds to the MH state is due to the fact that the information lies within the diffuse scattering. Here the MX-Chain compound  $[\text{Pd}(\text{cptn})_2\text{Br}]\text{Br}_2$  was studied by analyzing qualitatively and quantitatively the 3D- $\Delta$ PDF maps that unambiguously show that 2D sheets in CDW states are formed. It also reveals that the ordering of one given sheet is only slightly correlated with the ordering of the adjacent ones. The apparent discrepancy between different experimental methods pointing in diverse directions, *i.e.*, MH or CDW is explained. The formation of large macroscopic CDW domains, as observed in previous optical measurements[14] is the consequence of the very strong 2D hydrogen-bonding network that is formed between the ligand in the chain and the counteranion that links any two chains. We also showed that the small correlation between two different planes is mediated by the weak bond between the tip of the ligand ( $\text{CH}_2$  group) and the counteranion ( $\text{Br}^-$ ). From a chemistry point of view, this shows the importance of selecting the right ingredients in order to reduce or enhance those interactions and tune the physical properties of the material such as the conductivity. Recently, a multiple hydrogen-bonding network was used to enhance the electrical conductivity or form a conductive zigzag chain.[27-29] The CDW dimensionality can be designed based on the strength of those interactions, which can be quantitatively

measured by refinement of the disorder model. As examples of sophisticated chemical synthesis, the incorporation of aromatic in-plane ligands leads to the stabilization of the 1D chain structure in Pt-based MX-Chains,[30] the 2D hydrogen-bonding network gives the 2D-CDW in this study, and the fastener effect acting between alkyl chains leads to a phase transition between 3D CDW and MH state.[31,32] This 2D-CDW can totally be suppressed by synthesizing with a racemic mixture of cptn ligands, as this destabilizes the hydrogen-bonding network. The quantitative analysis using the software Yell showed that the displacement of the in-chain  $\text{Br}^-$  anion is in complete agreement with the empirical formula found for other Pd-based MX-Chains in the CDW state (Figure S7).[27] The advances in noise-free detector technology and highly intense X-ray beams permit the measurement of very high-quality reciprocal space mapping in a few minutes, thus allowing the research on quantitative analysis of diffuse scattering to progress and determine quantitative and meaningful structural parameters.[33-35] The 3D- $\Delta$ PDF method can be applied to a long list of low dimensional systems, from 1D molecular conductors[1-10,36,37] to 2D metal dichalcogenides[38] to solve their long-range and short-range structure.

## Experimental Section

**Data collection.** A set of single crystals of  $[\text{Pd}(\text{cptn})_2\text{Br}]\text{Br}_2$  of plate-like shape, with lateral dimensions of the order of some hundreds of  $\mu\text{m}$  were studied by X-Ray diffraction in a temperature range of 100-260 K. The SuperNova diffractometer (Agilent Technologies, UK) was employed to perform the measurements. A Cu anode source with voltage of 50 kV and a current of 50 mA were employed. Each image was  $1^\circ$  rotation and 1 s exposure. The CCD detector was positioned a distance of 60 mm.

**Structure determination procedure.** In addition to the structure solution presented in the introduction which was limited due to the use of a single axis diffractometer, conventional diffraction on a SuperNova diffractometer was conducted at 230K in order to increase redundancies and completeness. Structure solution and refinement via SHELXS and SHELXL respectively yielded an Orthorhombic structure of space group  $I222$ , with lattice parameters  $a = 5.247 \text{ \AA}$ ,  $b = 6.9646 \text{ \AA}$ ,  $c = 22.702 \text{ \AA}$  at 230 K. The structure consists of a body-centred arrangement of  $[\text{Pd}(\text{cptn})_2\text{Br}]\text{Br}_2$  chains. A single chain is composed an alternation of  $\text{Pd}(\text{cptn})_2$  units bridged by Br ions running along the  $a$  axis (Figure S3); the amine ( $\text{NH}_2$ ) groups of the (cptn) ligand provide cohesion between chains in the  $b$  direction through hydrogen bonds formed with the  $\text{Br}^-$  counteranions (Figure S5). The (cptn) ligands extend from each chain in the  $c$  direction (Figure S4). The space group  $I222$  was discriminated from its crystallographically indistinguishable counterpart  $Immm$  based on chemical reasons; the pentane group present in the ethylenediamine ligand is incompatible with  $mmm$  symmetry. The variation of the lattice parameters and Atomic Displacement Parameters (ADPs) with temperature was studied, and showed no evidence of any effect apart from the expected thermal expansion.

**Diffuse scattering data collection.** A set of single crystals of  $[\text{Pd}(\text{cptn})_2\text{Br}]\text{Br}_2$  of plate-like shape, with lateral dimensions of some hundreds of  $\mu\text{m}$ , were studied by X-Ray diffraction at 260 K to investigate the diffuse scattering. X-ray measurements were carried out at the Swiss Norwegian Beamline BM01 at the European Synchrotron Research Facility using monochromatized  $\lambda = 0.6973 \text{ \AA}$  X-rays. 900 images with 0.4 s exposure times and  $0.4^\circ$  step sizes were collected with a Pilatus2M detector located 247 mm downstream of the crystal. Short 3min data acquisition were performed every 20 K from 100K to 260K. Crystal were cooled using a Nitrogen gas flow cryosystem.

**Data reduction – XDS.** The structure solved is used a starting point to perform the already outlined steps of data reduction with the program XDS (MPI for Medical Research, Heidelberg). XDS applies the relevant instrumental corrections to the data, finds and indexes Bragg spots, determines the orientation matrix, integrates and corrects the measured intensities.

**Reconstruction of reciprocal space.** The orientation matrix as output from XDS is used to reconstruct the probed reciprocal space volume via a custom-made python script. The volume is a 3D array composed of  $801 \times 801 \times 801$  pixels. Each pixel corresponds to a step in  $h$ ;  $k$ ;  $l$  of 0.02, 0.03, and 0.08, respectively. The maximum indexes in the three directions are thus  $h = 9$ ,  $k = 12$ ,  $l = 32$ .

**Extraction of the diffuse scattering.** Considering the streak positions, a cubic volume is defined around each streak. The remaining portion of reconstructed space which is not contained in the cubic volume is artificially assigned a value of 0. Integration of the intensity contained in the cubic volume is then performed in

the  $h$  and  $k$  directions; moreover, averaging over the symmetry of the pattern is performed. Taking only the portions of the array which have a finite pixel value, a new array of size of  $18 \times 24 \times 800$  is constructed.

**Fourier Transform, PDF analysis and modelling.** The Fourier transform of this array is computed via the FFT algorithm of the Numpy library (Figure S6). The FT of the diffuse intensity is the 3D- $\Delta$ PDF of the probed crystal. The PDF is inspected to acquire insights into the disorder present in the sample, so to prepare a model to be refined with the software Yell. This software allows for the specification of a disorder model, starting from the average structure of the crystal (as determined previously). A set of variables corresponding to the parameters quantifying the different kinds of correlations (represented by the green arrow in Figure S6) is then added to the input file to simulate the effects of disorder on the average structure. The disordered model is then used to generate a  $\Delta$ PDF which is refined against the experimentally obtained one. The outcome of the refinement is thus a value for the correlation parameters which were included in the disorder model. The outcome of such calculation is shown in Figure S6.

## Author Contributions

L.G., S.T. and M.Y. coordinated the project; Crystals of  $[\text{Pd}(\text{cptn})_2\text{Br}]\text{Br}_2$  have been characterized and synthesized by T.Y., H.I. and S.T.; L.G., T.Y. and B.T. performed diffuse scattering measurements at ESRF with help of D.C.; L.G., A.S., E.Z. developed the data reduction procedure. L.G. wrote the manuscript with significant contributions from T.Y. and help from all authors.

## Note

The authors declare no competing financial interest.

## Acknowledgements

This project was carried out in the frame of the IM-LED LIA (CNRS) and Université de Rennes 1 – Tohoku University international joint program. This work was also partially supported by JSPS KAKENHI (19H05631). M. Y. thanks the support from the 111 project(B18030) from China. We thank Shun-Ichiro Tanaka, Elzbieta Trzop, Philippe Rabiller and Hervé Cailleau for their support.

**Keywords:** 3D- $\Delta$ PDF •MX chain • Charge-Density-Wave

- [1] J.P. Pouget, *Z. Kristallogr.* **2004**, *219*, 711-718
- [2] S. Ravy, *Annu. Rep. Prog. Chem., Sect. C: Phys. Chem.* **2007**, *103*, 223-260
- [3] J.P. Pouget, S. K. Khanna, F. Denoyer, R. Comès, A. F. Garito, A. J. Heeger, *Phys. Rev. Lett.* **1976**, *37*, 437-440
- [4] S. van Smaalen, *Acta Cryst.* **2005**, *A61*, 51-61
- [5] R. Kato, H. Cui, *Crystals* **2012**, *2*, 861-874
- [6] M. Buron-Le Cointe, M. H. Lemée-Cailleau, H. Cailleau, S. Ravy, J. F. Bélar, S. Rouzière, E. Elkaïm, and E. Collet, *Phys. Rev. Lett.* **2006**, *96*, 205503
- [7] H. Cui, T. Tsumuraya, H. H.-M. Yeung, C. S. Coates, M. R. Warren, R. Kato, *Molecules* **2019**, *24*(10), 1843

- 
- [8] L. Guérin, J. Hébert, M. Buron-Le Cointe, S.-I. Adachi, S.-y. Koshihara, H. Cailleau, and E. Collet, *Phys. Rev. Lett.* **2010**, *105*, 246101
- [9] T. Ishikawa, S. A. Hayes, S. Keskin, G. Corthey, M. Hada, K. Pichugin, A. Marx, J. Hirscht, K. Shionuma, K. Onda, Y. Okimoto, S. Koshihara, T. Yamamoto, H. B. Cui, M. Nomura, Y. Oshima, M. A. Jawad, R. Kato, R. J. D. Miller, *Science*, **2015**, *350*, 1501-1505
- [10] J.P. Pouget, *Crystals* **2012**, *2*(2), 466-520
- [11] M. Yamashita and H. Okamoto. *Material Designs and New Physical Properties in MX- and MMX-Chain Compounds*. Springer, **2013**
- [12] K. Nasu, *J. Phys. Soc. Jpn.* **1983**, *52*, 3865
- [13] S. Takaishi, M. Takamura, T. Kajiwara, H. Miyasaka, M. Yamashita, M. Iwata, H. Matsuzaki, H. Okamoto, H. Tanaka, S. Kuroda, H. Nishikawa, H. Oshio, K. Kato and M. Takata, *J. Am. Chem. Soc.* **2008**, *130*, 12080
- [14] T. Yoshida, S. Takaishi, H. Iguchi, H. Okamoto, H. Tanaka, S. Kuroda, Y. Hosomi, S. Yoshida, H. Shigekawa, T. Kojima, H. Ohtsu, M. Kawano, B. K. Breedlove, L. Guérin and M. Yamashita, *ChemistrySelect* **2016**, *2*, 259
- [15] Y. Wakabayashi, N. Wakabayashi, M. Yamashita, T. Manabe, N. Matsushita, *J. Phys. Soc. Jpn.* **1999**, *68*, 3948
- [16] V. Dyadkin, Ph. Pattison, V. Dmitriev, D. Chernyshov, *J. Synchrotron Rad.* **2016**, *23*, 3
- [17] T. R. Welberry and B. D. Butler. *Chem. Rev.* **1995**, *95*, 2369
- [18] T. R. Welberry, T. Weber, *Crystallography Reviews* **2016**, *22*(1), 2-78
- [19] M. E Wall, A. M Wolff, J. S Fraser, *Curr. Opin. Struct. Biol.* **2018**, *50*, 109-116
- [20] H. Sawa, *IUCrJ* **2016**, *3*, 298
- [21] T. Weber, A. Simonov. *Z. Kristallographie* **2012**, *227*, 238-247
- [22] A. Simonov. PhD thesis, ETH-Zurich, **2014**
- [23] A. Simonov, T. De Baeremaeker, H.L. Boström, et al. *Nature* **2020**, *578*, 256-260
- [24] D. Phelan, M. J. Krogstad, N. J. Schreiber, R. Osborn, A. H. Said, H. Zheng, and S. Rosenkranz, *Phys. Rev. B* **2019**, *100*, 054101
- [25] K. A. U. Holm, N. Roth, C. M. Zeuthen, K. Tolborg, A. A. Feidenhans'l and B. B. Iversen, *Phys. Rev. B* **2020**, *102*, 024112
- [26] A. Simonov, T. Weber, and W. Steurer, *Journal of Applied Crystallography* **2014**, *47*, 1146-1152
- [27] M Rasel Mian, H Iguchi, S Takaishi, U Afrin, T Miyamoto, H Okamoto, M Yamashita, *Inorg. Chem.* **2019**, *58*:114-120
- [28] M. Rasel Mian, U. Afrin, H. Iguchi, S. Takaishi, T. Yoshida, T. Miyamoto, H. Okamoto, H. Tanaka, S.-i. Kuroda, M. Yamashita, *CrystEngComm* **2020**, *22*, 3999-4004
- [29] M. Rasel Mian, H. Iguchi, S. Takaishi, H. Murasugi, T. Miyamoto, H. Okamoto, H. Tanaka, S.-i. Kuroda, B. K. Breedlove, M. Yamashita, *J. Am. Chem. Soc.* **2017**, *139*, 6562-6565
- [30] U. Afrin, H. Iguchi, M. Rasel Mian, S. Takaishi, H. Yamakawa, T. Terashige, T. Miyamoto, H. Okamoto, M. Yamashita, *Dalton Trans.* **2019**, *48*, 7828-7834
- [31] S. Takaishi, M. Takamura, T. Kajiwara, H. Miyasaka, M. Yamashita, M. Iwata, H. Matsuzaki, H. Okamoto, H. Tanaka, S. Kuroda, H. Nishikawa, H. Oshio, K. Kato, M. Takata, *J. Am. Chem. Soc.* **2008**, *130*, 12080-12084
- [32] M. Yamashita, *Bull. Chem. Soc. Jpn.* **2021**, *94*, 209-264
- [35] D. A. Keen, *Crystallography Reviews* **2020**, *26*, 143-201
- [34] T. Weber, H. B. Bürgi, *Acta Crystallogr. A.* **2002**, *58*(Pt 6):526-40
- [35] E. M. Schmidt, Reinhard B. Neder, *Phys. Rev. B* **2019**, *100*, 054201
- [36] K. Otsubo, H. Kitagawa, *CrystEngComm* **2014**, *16*, 6277-6286
- [37] Y. Yoshida, H. Kitagawa, *Chem. Commun.* **2020**, *56*, 10100-10112
- [38] K. Nakatsugawa, S. Tanda, T.N Ikeda, *Sci. Rep.* **2020**, *10*, 1239

